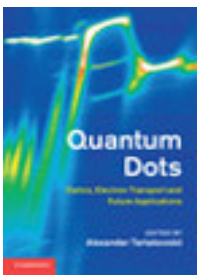

Quantum Dots

Optics, Electron Transport and Future Applications

Edited by Alexander Tartakovskii

Book DOI: http://dx.doi.org/10.1017/CBO9780511998331

Online ISBN: 9780511998331

Hardback ISBN: 9781107012585

Chapter

9 - Quantum dots in photonic crystal cavities pp. 153-168

Chapter DOI: http://dx.doi.org/10.1017/CBO9780511998331.010

Cambridge University Press

9

Quantum dots in photonic crystal cavities

A. Faraon, D. Englund, I. Fushman, A. Majumdar and J. Vučković

9.1 Introduction

During the past two decades, the development of micro- and nano-fabrication technologies has positively impacted multiple areas of science and engineering. In the photonics community, these technologies had numerous early adopters, which led to photonic devices that exhibit features at the nano-scale and operate at the most fundamental level of light–matter interaction [28, 39, 18, 29]. One of the leading platforms for these types of devices is based on gallium arsenide (GaAs) planar photonic crystals (PC) with embedded indium arsenide (InAs) quantum dots (QDs). The PC architecture is advantageous because it enables monolithic fabrication of photonic networks for efficient routing of light signals of the chip [26]. At the same time, PC devices have low loss and ultra-small optical mode volumes, which enable strong light–matter interactions. The InAs quantum dots are well suited for quantum photonic applications because they have excellent quantum efficiencies, large dipole moments, and a variety of quantum states that can be optically controlled [24, 3].

Currently, the development of these photonic technologies is geared mainly towards applications in quantum and classical information processing. The first proposals for quantum information processing using QDs in optical microresonators were developed more than a decade ago in the broader context of quantum information processing using quantum systems (such as atoms, ion, molecules) that can be optically controlled [23, 17]. Compared to other systems, the solid-state quantum photonic platform is attractive for quantum information applications because of its potential for large-scale integration [27]. For classical information processing these technologies are relevant because of the continuous drive to develop devices that have smaller footprint and operate at lower power [25]. In this respect, PCs with coupled QDs approach a fundamental limit, where light is confined in a region on the order of one cubic optical wavelength and the optically active material operates at the level of one quantum of excitation. This enables devices that can switch light at the single photon level and consume minute amounts of energy during operation.

Quantum Dots: Optics, Electron Transport and Future Applications, ed. Alexander Tartakovskii. Published by Cambridge University Press.

In this chapter we give an overview of our recent work on developing quantum photonic devices based on the QD–PC platform. Section 9.2 is a brief introduction to QDs, PCs, and the formalism to analyze coupled cavity/QD systems. In Section 9.3 we summarize the main experimental techniques utilized for fabrication, optical probing and tuning of these devices. In Section 9.4 we discuss how these techniques are used to probe strongly coupled QDs, and in Section 9.5 we focus on optical nonlinearities at the single photon level that are present in these systems. In the last section (Section 9.6) we comment on applications and future directions.

9.2 Quantum dots and photonic crystals

9.2.1 InAs quantum dots

Semiconductor QDs are nano-scale inclusions of a low-bandgap semiconductor inside a semiconductor with a larger bandgap. The bandgap difference acts as a potential barrier for carriers (electrons and holes), confining them inside the dot. Moreover, the dots are small enough (nanometer size) that the confined carriers can occupy only discrete energy levels, and the transitions between such levels in the conduction band and the valence band involve the absorption or emission of photons at optical frequencies. QDs can be formed spontaneously during epitaxial growth of lattice-mismatched materials, and such dots are called self-assembled [24]. For example, when InAs is deposited on GaAs, a strained planar layer, known as a wetting layer, initially forms. The strain energy that builds up in this layer is eventually partially relieved by the formation of nanometer-scale islands on the surface, which can subsequently be covered with a capping layer of GaAs.

InAs/GaAs QDs used in our experiments were self-assembled during molecular beam epitaxy (MBE), under conditions that give relatively sparse dots, with a surface density of $\sim 100\,\mu\mathrm{m}^{-2}$. These QDs are engineered to emit at near infrared wavelengths ($\approx 930\,\mathrm{nm}$) when operating at cryogenic temperatures (below $\approx 50\,\mathrm{K}$) as discussed in Section 9.3.2. A typical spectrum of an ensemble of QDs is shown in Fig. 9.1a together with an atomic force microscope image (Fig. 9.1b) taken before the growth of the GaAs capping layer. These QDs self-assemble at random locations on the surface of the wafer.

9.2.2 Photonic crystals

Photonic crystals are formed by periodic arrangements of optical media with various refractive indexes [19]. The light in such structures is controlled via distributed Bragg reflection (DBR), that allows for the development of photonic bandgaps analogous to the electronic bandgaps in semiconductors. In such a material and at frequencies inside the photonic bandgap, the propagation of light is prohibited in all crystal directions. The 2D PCs drew most attention because they can be fabricated in a monolithic fashion using techniques already well developed in the semiconductor industry. The most common form for

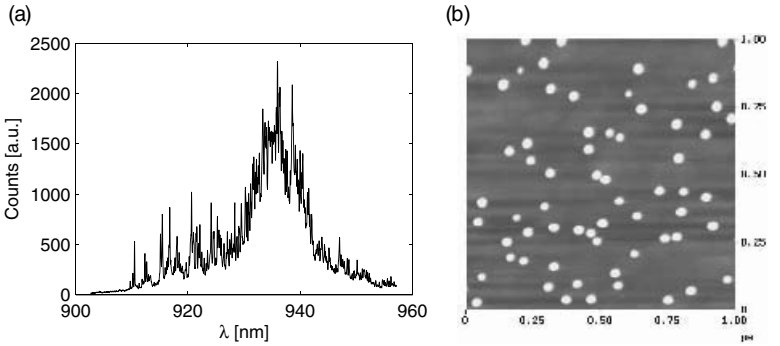

Figure 9.1 (a) Spectrum of an ensemble of QDs showing an inhomogeneous broadening of ≈ 20 nm. (b) Atomic force microscope image of QDs (un-capped) showing their random spatial distribution on the GaAs wafer (Image courtesy of Dr. Bingyang Zhang, Stanford University).

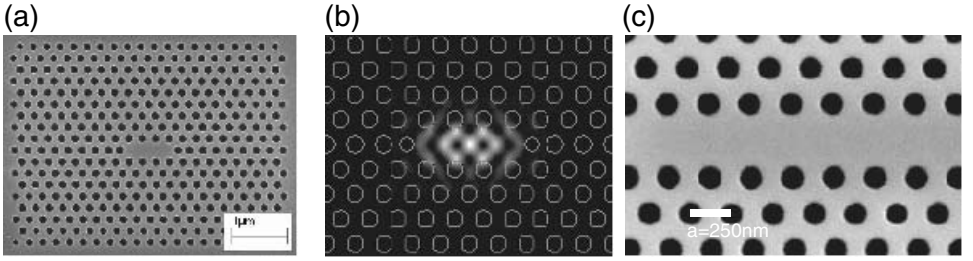

Figure 9.2 (a) Scanning electron microscope image of a linear three hole defect cavity fabricated in a 160 nm thick GaAs slab. (b) Simulated electric field intensity of the fundamental mode. (c) Fabricated W1 waveguide.

2D PCs is a periodic lattice (triangular of square) of holes patterned in a thin suspended membrane of high refractive-index material (n).

The confinement of light can be achieved by introducing perturbations into the periodicity of the photonic lattice, which leads to formation of PC cavities. The two main parameters used to characterize these cavities are the quality factor and the mode volume. The quality factor is defined as $Q = \lambda/\Delta\lambda$, with λ the wavelength in vacuum and $\Delta\lambda$ the cavity resonance linewidth, and V is defined in Section 9.2.3. Most of the results reported in this chapter were obtained using linear three-hole defect cavities (L3) [1]. A scanning electron microscope (SEM) image of a L3 cavity fabricated in GaAs is shown in Fig. 9.2, together with the profile (simulation) of the electric field intensity in the fundamental mode. The mode is TE (transversal electric)-like with the electric field polarized primarily in the PC plane. The design of the cavity can be engineered such that this mode can reach quality factors on the order of hundreds of thousands and optical mode volumes smaller than one cubic optical wavelength. The L3 cavity can be easily connected in a photonic network using PC waveguides. We used W1 waveguides created by omitting a row of holes in the triangular lattice (Fig. 9.2c).

9.2.3 Physics of quantum dots in photonic crystal cavities

Let us assume that a single QD is located inside a PC cavity and thus coupled to the cavity field. We also assume that the transition frequency (ω_{QD}) from the one-exciton (i.e. an electron–hole pair trapped in the QD) state $|e\rangle$ to the zero-exciton state $|g\rangle$ is on resonance or nearly on resonance with the fundamental optical cavity mode frequency ω_c. Under these conditions, the excitation of other cavity modes can be neglected, and the system can be modeled as a single two-level atom coupled to a single cavity mode. This coupled system can be described by the Jaynes–Cummings Hamiltonian [35, 41]:

$$H = H_E + H_F + H_I\,, \tag{9.1}$$

where $H_E = \hbar\omega_{QD}\sigma_z$, $H_F = \hbar\omega_c\left(a^\dagger a + \frac{1}{2}\right)$ and $H_I = i\hbar\left(g(\vec{r}_E)a^\dagger\sigma_- - g^*(\vec{r}_E)\sigma_+ a\right)$.

The three terms of the Jaynes–Cummings Hamiltonian are the excitonic Hamiltonian (H_E), the field Hamiltonian (H_F), and the exciton–field interaction Hamiltonian (H_I); a and $a^\dagger$ are the photon annihilation and creation operators, respectively, $\sigma_- = |g\rangle\langle e|$ and $\sigma_+ = |e\rangle\langle g|$ are the QD lowering and raising operators, respectively, while $\sigma_z = \frac{1}{2}\left(|e\rangle\langle e| - |g\rangle\langle g|\right)$ is the population operator. The coupling parameter $g(\vec{r}) = g_0\psi(\vec{r})\cos(\xi)$ is the product of the Rabi frequency $g_0 = \frac{\mu}{\hbar}\sqrt{\frac{\hbar\omega_c}{2\epsilon_M V}}$, a position-dependent part $\psi(\vec{r}) = \frac{E(\vec{r})}{|E(\vec{r}_M)|}$, and a polarization-dependent part $\cos(\xi) = \frac{\vec{\mu}\cdot\hat{e}}{\mu}$, where $\vec{r}_M$ denotes the point where the field intensity $\epsilon(\vec{r})|E(\vec{r})|^2$ is maximum and ϵ_M is the dielectric constant at this point ($\epsilon_M = \epsilon(\vec{r}_M)$). Electric field orientation at the location $\vec{r}$ is denoted as $\hat{e}$, $\vec{\mu}$ is the dipole moment matrix element between the states $|e\rangle$ and $|g\rangle$, and $\mu = |\vec{\mu}|$. Note that $\vec{\mu}$ is defined as $q\langle e|\vec{d}|g\rangle$, where $\vec{d}$ is the coordinate operator and q is a unit charge; $g(\vec{r}_E)$ denotes the value of the coupling parameter at the QD exciton location $\vec{r}_E$, and $|g(\vec{r}_E)|$ reaches its maximum value of $|g_0|$ when the exciton is located at the point $\vec{r}_M$ where the field intensity is maximum, and when its dipole moment is aligned with the electric field (i.e. when $\psi(\vec{r}_E) = 1$ and $\cos(\xi) = 1$). $E(\vec{r})$ is the electric field magnitude, and V is the cavity mode volume, defined as $V = \frac{\int\int\int \epsilon(\vec{r})|E(\vec{r})|^2 d^3\vec{r}}{\epsilon_M|E(\vec{r}_M)|^2}$. Note that H_I can be derived from the interaction Hamiltonian in the dipole approximation ($H_I = -\vec{\mu}\cdot\vec{E}$), after the expansion and quantization of electric field in terms of the cavity modes.

The losses of the system can be described in terms of the *cavity field decay rate* κ, equal to ($\omega_c/2Q$), and the *excitonic dipole decay rate* γ; κ is the decay rate of the resonant cavity mode, while γ includes losses to modes other than the cavity mode and to nonradiative decay routes. With losses taken into account, the eigenstates of the system Hamiltonian are:

$$\omega_\pm = \frac{\omega_c + \omega_{QD}}{2} - i\frac{\kappa+\gamma}{2} \pm \sqrt{g^2 + \frac{1}{4}\left(\delta - i(\kappa-\gamma)\right)^2}, \tag{9.2}$$

where $\delta = \omega_{QD} - \omega_c$ is the QD/cavity detuning. Depending on the ratio of the coupling parameter $|g(\vec{r}_E)|$ to the decay rates κ and γ, we can distinguish two regimes of coupling between the exciton and the cavity field. For $\delta = 0$ and $\kappa >> \gamma$ (typical for our regime of operation) the system eigenstates are degenerate (i.e. real parts of the two solutions of

Eq. (9.2) are equal) for $g < \kappa/2$ (*weak coupling regime*) and non-degenerate with splitting $\sim 2g$ for $g > \kappa/2$ (*strong coupling regime*) [20]. In the strong-coupling case, the time scale of coherent coupling between the exciton and the cavity field is shorter than that of the irreversible decay into various radiative and nonradiative routes. *Rabi oscillation* occurs in this case, and (in the weak excitation limit) the time evolution of the system can be described by oscillations at frequency $2|g(\vec{r}_E)|$ between the states $|e, 0\rangle$ and $|g, 1\rangle$, where $|e, 0\rangle$ corresponds to one exciton in the QD and no photons in the cavity, and $|g, 1\rangle$ corresponds to zero excitons in the QD and one photon in the cavity. On the other hand, in the weak-coupling case, the irreversible decay rates dominate over the coherent coupling rate; in other words, the exciton–cavity field system does not have enough time to couple coherently before dissipation occurs.

Operation both in strong- and weak-coupling regimes has important consequences on the emission properties of the QD and the transmission properties of the coupled cavity/QD system. In the weak-coupling regime, the emission rate of the QD can be strongly enhanced via the Purcell effect [32] which is relevant for single-photon sources [33]. In this chapter we focus mainly on how the coupling of a single QD can modify the amplitude and the quantum statistics of coherent light transmitted through the cavity. In the weak-interaction limit excitation limit (when the average number of photons in the cavity is much smaller than one per cavity photon lifetime), the optical transmission function is given by the following formula:

$$T = \eta \left| \frac{\kappa}{i(\omega_c - \omega) + \kappa + \frac{g^2}{i(\omega_{QD} - \omega) + \gamma}} \right|^2, \tag{9.3}$$

where ω is the probe frequency, and η is a scaling factor that depends on the coupling efficiency of light into the cavity [6].

For typical parameters found experimentally in GaAs photonic crystal cavities coupled to InAs QDs ($\kappa/2\pi = 16GHz, \gamma/2\pi \sim 0.1GHz$), the normalized transmission function is shown in Fig. 9.3. What makes this system remarkable is that the presence of the coupled dipole can change the system from fully transparent to opaque even for modest values of the coupling rate g when the system is not in the strong-coupling regime [40]. This simple property is essential for implementing quantum repeaters for quantum information processing [40], or basic optoelectronic switches that operate at ultra-low energy levels. For switching applications the frequency of the quantum emitter can be controlled using external factors as local electric fields [12] or other optical fields [13].

9.3 Experimental techniques

9.3.1 Fabrication techniques

In our experiments, PCs are typically fabricated in 160 nm thick GaAs membranes grown by molecular beam epitaxy (MBE) on top of an $Al_xGa_{1-x}As$ sacrificial layer. The thickness is chosen to match half the QD emission wavelength ($\sim \lambda/2n$, where n is the GaAs

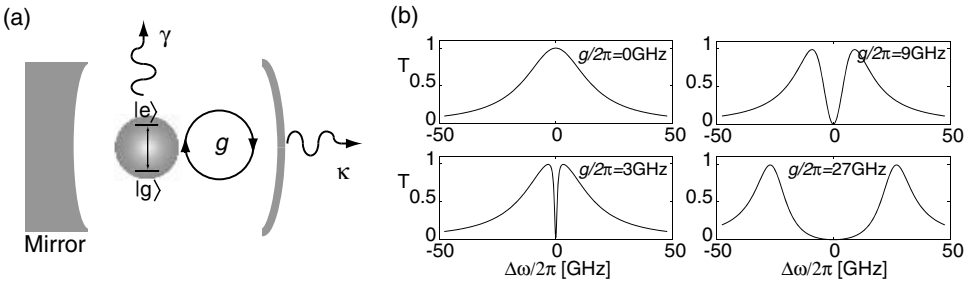

Figure 9.3 (a) Schematic representation of a one-sided optical cavity with a coupled optical dipole. The dipole couples to the cavity mode with rate g, the cavity field decay rate is κ and the spontaneous emission rate of the dipole is γ. (b) Theoretical transmission spectra of a coupled cavity/QD system ($\kappa/2\pi = 16\,GHz$, $\gamma/2\pi = 0.1\,GHz$) for different values of the coupling constant g. These spectra indicate that the transmission function of the cavity is significantly affected by the presence of the dipole even in the weak-coupling regime ($g < \kappa/2$)

refractive index). The membranes contain a QD layer in the middle. A distributed Bragg reflector (DBR) consisting of an AlAs/GaAs quarter wave stack was grown under the sacrificial layer. The DBR reflects all the light scattered from the QD into the GaAs substrate, thus improving collection efficiency in the out-of-plane direction.

The PCs are made using electron beam lithography and dry plasma etching. The pattern is first defined in the electron beam resist that is further used as an etch mask for the GaAs membrane. After patterning, the sacrificial layer is removed using wet etching, which results in suspended PC membranes. The concentration of Al in the sacrificial $Al_xGa_{1-x}As$ layer (x) can vary, depending on the desired wet etching rate (our best results were obtained with $x = 0.8$). Beside these basic semiconductor processing techniques, other steps may be required for more sophisticated devices involving electrical contacting or tuning.

9.3.2 Optical probing methods

During experiments, the sample is placed inside an optically accessible liquid-helium flow cryostat that maintains temperatures under 50 K. The optical measurement is done with a microscope setup. This type of setup, schematically shown in Fig. 9.4, uses the same lens both for focusing the probe light onto the sample and for collection of the output signal. In the case of resonant measurements, where the input and output signals have similar wavelengths, a cross-polarized configuration implemented using a polarizing beam splitter can be an efficient way to filter the output signal from the direct reflection of the input beam [6]. At the same time, wave-plates can be used to control the polarization of light incident on the sample and filters can be added in the output path to collect only part of the spectrum. The output signal can be sent to various measuring instruments (i.e. spectrometer, imaging camera, streak camera, photon counters) depending on the specific application.

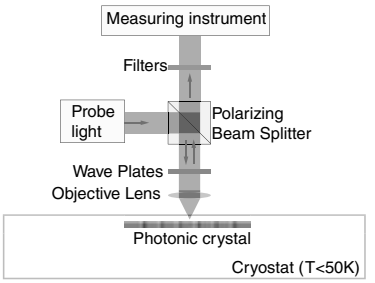

Figure 9.4 Schematic representation of an optical measurement setup used to probe photonic crystal cavities. Figure adapted from Ref. [12].

Depending on the wavelength of the probe light used to excite the QDs, there are two types of measurement: photoluminescence measurements and resonant measurements. In photoluminescence, the probe light excites free carriers that randomly recombine in the QD with the emission of photons that can be collected and measured. For this type of measurement, the probe is generally tuned above the GaAs bandgap. For resonant measurements, the probe is tuned on resonance with the cavity or the QD frequency.

9.3.3 Tuning and positioning techniques

As discussed in previous sections, InAs QDs have great advantages that make them excellent candidates for studying solid-state cavity quantum electrodynamics (CQED). However, one of the main drawbacks is their spectral inhomogeneous broadening and randomness in their spatial location (Fig. 9.1). This is caused by the limited amount of control over the self assembling process during the MBE growth. To overcome this difficulty, several frequency tuning and positioning techniques have been developed.

For frequency matching, the resonance of either the QD or the cavity can be controlled. One of the most common techniques to tune QDs and cavities into resonance is to change the temperature of the entire chip simply by controlling the temperature of the cryostat. The bandgap of both GaAs and InAs changes with temperature thus resulting in a shift of the QD emission lines. QDs can experience a red shift in their resonance of a couple of nanometers when temperature is changed from 4 K to about 50 K. At the same time, the cavity resonance is sensitive to temperature because of changes in the refractive index. Over the same temperature interval, the cavity resonance changes at a rate that is roughly three times slower than that of the QD.

Changing the temperature of the entire cryostat has some limitations: it is slow and all devices on the same chip are tuned at the same time. To overcome this difficulty, we developed local temperature tuning techniques that greatly improve the tuning speed and allow for simultaneous tuning of different cavities and QDs on the same chip [9]. Local temperature tuning was implemented by using the device shown in Fig. 9.5a whose temperature

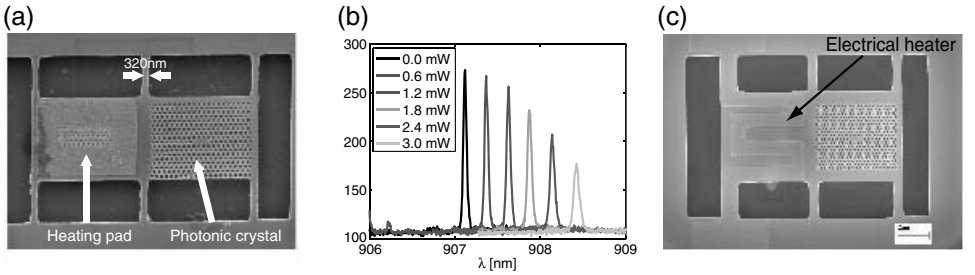

Figure 9.5 (a) Suspended structure with PC cavity and a metal-coated heating pad, used for local temperature tuning. (b) Local temperature tuning of a QD line while the power of the heating laser (measured before the focusing lens) was changed from 0 to 3 mW. (c) Scanning electron microscope of a PC structure equipped with a micron-scale electrical heater that can be used locally to control the temperature of the device. Figures adapted from Refs. [8, 9].

can be controlled via an external laser beam. The external laser was focused on a metal-coated heating pad located next to the cavity. The performance of the technique is shown in Fig. 9.5a, where a single QD line is tuned by up to 1.5 nm.

For larger-scale integration, where multiple components need to be controlled independently, it may be necessary for the temperature to be controlled via electrical heaters as demonstrated in Faraon and Vuckovic [8]. A prototype device that can be controlled in this way is shown in Fig. 9.5c. The temperature of devices of this type was controlled at speeds as high as 100 kHz, limited by the thermal relaxation time of the device.

Local temperature tuning provides fast and reliable control of the cavity and QD resonance. However, since both the resonator and the QD resonance depend on temperature, the technique does not provide enough control to tune into resonance several QDs and cavities on the same chip, as needed for future quantum networks. One solution may be a second local tuning technique that allows for fine control of the cavity resonance by using photorefractive materials [7]. The photorefractive material of choice was As_2S_3, a chalcogenide glass that changes its refractive index when excited with green light. Resonance shifts of up to 3 nm were observed for cavities resonant at 940 nm. During the tuning process the quality factor degraded from $Q \sim 7000$ to $Q \sim 4650$; however, the resulting Q is still sufficient to observe strong QD-cavity coupling.

The speed of the local temperature tuning techniques is limited by the thermal relaxation time of the PC device (typically below 1 MHz). For ultra-fast control, the QD can be modulated directly using electric fields [14] that modify the QD frequency via the quantum-confined Stark effect. We implemented [12] this type of control for QDs coupled to cavities (Fig. 9.6). A metallic electrode is placed next to the cavity such that it has a minimal overlap with the optical mode. When a bias voltage is applied, a depletion region and thus an electric field is created around the electrode. For voltages greater than $\sim 4\,V$ the depletion region reaches the QD in the cavity (Fig. 9.6b) and the QD experiences a frequency red shift. We were able to modulate the QD emission frequency up to speeds as

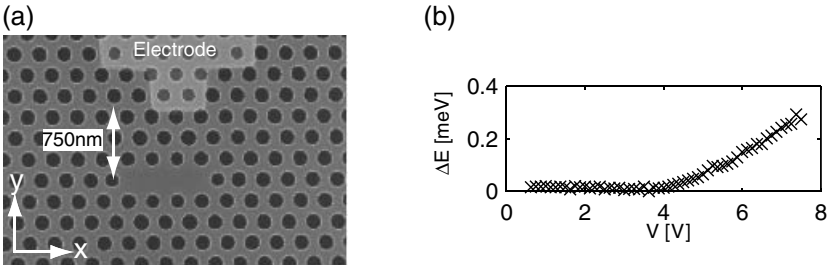

Figure 9.6 (a) Scanning electron microscope image of a PC cavity with a metallic electrode in close proximity. Electric fields can be created by applying a bias voltage on the electrode, thus tuning QDs coupled to the cavity. (b) Stark shift of a cavity-coupled QD as a function of the applied voltage. Figures adapted from Ref. [12].

high as 150 MHz (limited by the transmission line in the cryostat) but modulation speeds up to tens of GHz are possible using this method.

Beside the spectral alignment between the cavity and the QD, the second major challenge is the spatial alignment. During the MBE process, the QDs grow in random places on the wafer, which makes it difficult to fabricate the resonator such that it overlaps with the QD. For basic CQED experiments that employ a single cavity/QD system, it it possible to fabricate a large number of resonators and then search for one system where the cavity and the QD overlap [5, 42]. Another method developed by other groups is to precisely locate the position of the QD and then fabricate the resonator on top of it [15, 38]. In principle, this approach allows for more deterministic coupling of the QD to the cavity mode, and increases the likelihood that only a single QD is coupled to the cavity, but it is time consuming.

For more-complex devices that involve multiple QDs and cavities coupled in an on chip network, the alignment difficulty for all the techniques already described increases exponentially with the number of nodes in the network. Thus, to make this technology truly scalable, the QDs should be grown in predefined positions, which would solve the problem of spatial alignment. The spectral alignment could be done afterwards with local tuning techniques. There is an ongoing effort in growing QDs in predefined positions, but so far the radiative properties of these QDs did not match the ones of the self-assembled QDs [21, 34, 2, 43, 22].

9.4 Probing the strong-coupling regime

The strong-coupling regime occurs when the energy loss of the coupled cavity/QD system is low, such that a coherent back and forth energy transfer between the QD and the cavity mode can be sustained (see Section 9.2.3). Quantum mechanically, in this regime the states of the QD and the cavity become mixed into a new set of two eigenstates (with energies given by Eq. (9.2)) that have both cavity and QD character. One characteristic of systems in

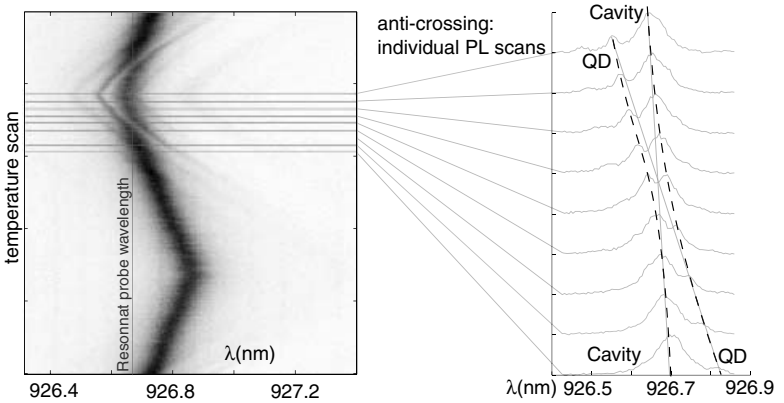

Figure 9.7 Cavity-QD anti-crossing in photoluminescence, a signature of the strong coupling regime, observed when tuning the QD across the cavity resonance using local temperature tuning. In the left panel the vertical axis represents the scan of the temperature with a triangular function. In the right panel, the dashed lines mark the wavelength of the polaritons, and the continuous lines mark the cavity and QD wavelength. Figures adapted from Refs. [6, 10].

the strong-coupling regime is that they should always display two spectral lines, regardless of the detuning between the cavity and the QD, a characteristic known as *anti-crossing* or *avoided crossing* of the spectral lines.

For QDs in micro-cavities, the anti-crossing can be easily observed in photoluminescence measurements as the QD is tuned on resonance with the cavity [42, 15, 30, 9]. The photoluminescence from a strongly coupled system is shown in Fig. 9.7 [6], where the tuning of the QD was done by local temperature tuning (see Section 9.3.3). The parameters of the system are: $\kappa/2\pi = 16$ GHz (linewidth 0.1 nm), Rabi frequency $g/2\pi = 8$ GHz (from Rabi splitting of $2g$ corresponding to 0.05nm), and $\gamma/2\pi \approx 0.1$ GHz. Since $g \approx \kappa/2$, the system operates on the onset of the strong-coupling regime where Rabi oscillations are only initiated, but a full oscillation is not completed.

Probing strong coupling via photoluminescence represents a very strong tool for characterization. However, for most applications the QDs-coupled cavities must be probed resonantly. Resonant probing enables the study of coherent interactions between the cavity, QD and laser fields. We reported resonant probing in Englund *et al.* [6], where the transmission function of the strongly coupled system shown in Fig. 9.7 was measured using a cross-polarized reflectivity measurement (see Section 9.3.2). For this measurement, the laser was kept at a constant resonant probe wavelength as marked in Fig. 9.7, while the cavity and QD were tuned using local temperature tuning. The expected intensity of the reflectivity signal is given by Eq. (9.3). When the QD is not coupled to the cavity (i.e. $g = 0$), the equation becomes the Lorentzian function that describes the transmission function of any resonator. A coupled QD ($g > 0$) will cause a drop in transmission (or reflectivity R) due to the coherent interaction with the laser and the cavity field. This

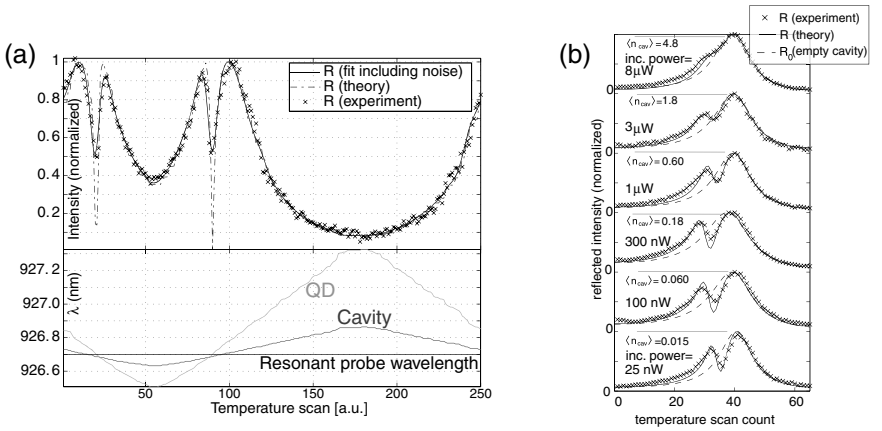

Figure 9.8 (a) Reflectivity spectrum as a function of the cavity/QD detuning. The bottom panel indicates the cavity, QD and probe laser wavelengths during the temperature tuning. (b) Dependence of the reflectivity spectrum with the incident power of the probe laser (measured before the objective lens). As the power is increased to levels above one photon per cavity lifetime ($\langle n_{cav} \rangle \sim 1$), the drop in reflectivity caused by the interaction with the QD vanishes. Figures adapted from Refs. [6, 10].

effect, shown in Fig. 9.8a, demonstrates that the transmission of a resonator can be controlled by using a single quantum emitter. This type of control is achieved for input optical powers corresponding to one photon per cavity lifetime (nanowatts). The system has ultrahigh optical nonlinearities and can be controlled with minute power levels as discussed in the next sections.

9.5 Nonlinear optics at the single photon level

9.5.1 Amplitude and phase nonlinearities

Single QDs in PC cavities cause dramatic changes in the transmission function of the resonator, as previously discussed in Section 9.4. Because of the nonlinearity of the system, these changes are strongly dependent on the power of the probe laser as shown in Fig. 9.8b. The reflectivity is shown for various incident powers of the probe laser and the corresponding average photon number in the cavity (n_{cav}). The saturation behavior is modeled using a steady-state solution of the quantum master equation (solid line) as described in Tan [36]. The dashed curve shows the reflectivity ratio if no thermal fluctuations were present. At large power, both curves tend to unity as the QD/cavity spectrum approaches the Lorentzian shape of the empty cavity.

This optical nonlinearity can be exploited to control both the transmission and the phase of light interacting with the cavity, with control energies at the single photon level. Experiments can be designed where the intensity and the phase of a probe laser resonant with the QD can be controlled via a second laser beam that is detuned from the QD frequency but

close enough to efficiently interact with it. This types of experiments on amplitude control and controlled phase shifts are reported in Fushman *et al.* [13]. The achievement of phase control using coupled QDs in cavities demonstrated the potential to use these systems to build control phase gates [37] as needed in optical quantum computing devices, and may enable optical quantum non-demolition measurements on a chip.

9.5.2 Photon blockade and photon-induced tunneling

The presence of a coupled QD in the cavity not only affects the amplitude and phase of the light transmitted or reflected from the resonator, but also affects its quantum statistics. While the laser light interacting with a empty resonator preserves its Poissonian statistics, when an optical emitter is strongly coupled to the cavity the scattered light can acquire non-classical character, either sub-Poissonian or super-Poissonian. This is the result of the interaction between the laser field and a quantum system that has eigenstates with anharmonic spacing.

In strong-coupling regimes, the energy eigenstates of the system are grouped in two-level manifolds with eigen-energies given by $n\omega_c \pm g\sqrt{n}$ (for $\omega_{QD} = \omega_c$), where n is the number of energy quanta in the cavity–QD system. The eigenstates can be written as:

$$|n, \pm\rangle = \frac{|g, n\rangle \pm |e, n-1\rangle}{\sqrt{2}}, \tag{9.4}$$

where $|g\rangle$ and $|e\rangle$ are the ground and excited states of the QD, and $|n\rangle$ is the photon number state of the optical mode. The energy splitting between the eigenstates in each manifold is nonlinear in n and given by $2g\sqrt{n}$ (Fig. 9.9). This anharmonicity in the splitting of the energy eigenstates gives rise to nonlinear optics phenomena at the single photon level, like photon blockade [16, 4] and photon-induced tunneling. In the case of photon blockade, the presence of one photon in the cavity blocks subsequent photons to enter the resonator. For example, let's consider that a coherent laser source is coupled to the cavity (Fig. 9.9a) and is resonant to one of the polaritons, say $|1, -\rangle$ (continuous arrow in Fig. 9.9b). Once a photon is coupled, the system is excited into the state $|1, -\rangle$, so the coupling of another photon with energy $\omega_c - g$ would require the system to transition to energy state $2(\omega_c - g)$. However, the system does not have an eigenstate at this energy, the closest being at $2\omega_c - g\sqrt{2}$, so the probability of coupling the second photon is reduced. Thus, it is preferential for only a single photon at at time to couple into the cavity and then to be emitted at the output port (sub-Poissonian statistics).

Another interesting regime of operation is photon-induced tunneling [10], when the laser is resonant with a n-photon transition to one of the levels in the nth order manifold ($\omega_c - g/\sqrt{n}$) (dashed arrow in Fig. 9.9b). In this case, coupling a single photon into the system has a low probability, but once a photon is coupled it becomes preferential for more photons to tunnel into the cavity to match the energy level in the nth order manifold. At the output port, it is more probable that photons exit in bunches (super-Poissonian statistics).

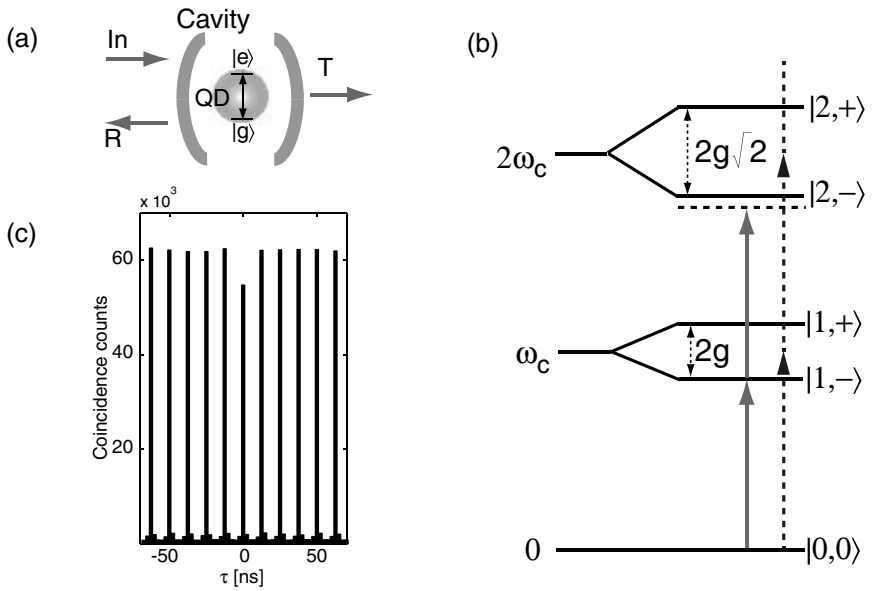

Figure 9.9 (a) Schematic representation of a single QD coupled to an optical resonator. (b) Anharmonic ladder of energy eigenstates for a strongly coupled cavity-QD system. The solid arrows indicate the one-photon transition to $|1,-\rangle$, while the dashed arrows indicate the n-photon transition (n large) to $|n,\pm\rangle$ (c) Measured second-order correlation data for laser pulses reflected from the cavity/QD system. The laser is tuned at the photon blockade frequency so photon anti-bunching is observed ($g^{(2)}(0) = 0.91$). Figures adapted from Refs. [6, 10].

These effects can be measured experimentally via second-order correlation measurements on the output field [10]. We probed photon blockade and photon-induced tunneling using laser pulses reflected from a strongly coupled cavity/QD system. The experimental data indicating photon anti-bunching (sub-Poissonian statistics) due to photon blockade are shown in Fig. 9.9c. The probing of photon blockade and photon-induced tunneling demonstrates optical nonlinearities at the single photon level in solid state systems. These types of nonlinearities open the possibility to develop deterministic sources of non-classical light and optical logic devices that operate at ultra-low power levels.

9.6 Applications and future directions

In the previous sections we discussed basic experiments that demonstrate how a QD strongly coupled to a cavity mode can be used to control both the amplitude and the quantum statistics of a light beam transmitted through the cavity. We also presented experimental techniques for local control of QDs and cavities on the chip. These experiments lay down the foundation for future quantum photonic devices. One example is the electro-optic switch based on a single QD that we recently developed [12]. The optical switching

in this devices occurs at the level of single photons interacting with single excitons, with minute energies required for the switching action. In terms of integration, we demonstrated devices where the cavity/QD system is connected to PC waveguides [11] and the QD is used to control the intensity of light transmitted into the waveguide. The next important challenge is to deterministically control the quantum spin states of a QD in a cavity [31] and also to integrate these devices into a complex photonic network as required for most applications in classical and quantum information processing.

References

[1] Akahane, Y., Asano, T., Song, B.-S. and Noda, S. 2003. High-Q photonic nanocavity in a two-dimensional photonic crystal. *Nature*, **425**(6961), 944–947.
[2] Atkinson, P., Ward, M. B., Bremner, S. P. *et al*. 2006. Site-control of inAs quantum dots using *ex-situ* electron-beam lithographic patterning of GaAs substrates. *Japanese Journal of Applied Physics*, **45**(4A), 2519–2521.
[3] Benson, O. and Henneberger, F. 2009. *Semiconductor Quantum Bits*. Pan Stanford Publishing.
[4] Birnbaum, K. M., Boca, A., Miller, R. *et al.* 2005. Photon blockade in an optical cavity with one trapped atom. *Nature*, **436**, 87–90.
[5] Englund, D., Fattal, D., Waks, E. *et al.* 2005. Controlling the spontaneous emission eate of single quantum dots in a two-dimensional photonic crystal. *Phys. Rev. Lett.*, **95**(013904).
[6] Englund, D., Faraon, A., Fushman, I. *et al.* 2007. Controlling cavity reflectivity with a single quantum dot. *Nature (London)*, **450**(7171), 857–861.
[7] Faraon, A., Englund, D., Bulla, D. *et al.* 2008a. Local tuning of photonic crystal cavities using chalcogenide glasses. *Appl. Phys. Lett.*, **92**(043123).
[8] Faraon, A. and Vučković, J. 2009. Local temperature control of photonic crystal devices via micron-scale electrical heaters. *Appl. Phys. Lett.*, **95**(4), 043102.
[9] Faraon, A., Englund, D., Fushman, I. *et al.* 2007. Local quantum dot tuning on photonic crystal chips. *Appl. Phys. Lett.*, **90**(213110), 213110.
[10] Faraon, A., Fushman, I., Englund, D. *et al.* 2008b. Coherent generation of non-classical light on a chip via photon-induced tunnelling and blockade. *Nature Physics*, **4**(11), 859–863.
[11] Faraon, A., Fushman, I., Englund, D. *et al.* 2008c. Dipole induced transparency in waveguide coupled photonic crystal cavities. *Optics Express*, **16**(16), 12154.
[12] Faraon, A., Majumdar, A., Kim, H., Petroff, P. and Vučković, J. 2010. Fast electrical control of a quantum dot strongly coupled to a photonic-crystal cavity. *Phys. Rev. Lett.*, **104**(4), 047402.
[13] Fushman, I., Englund, D., Faraon, A. 2008. Controlled phase shifts with a single quantum dot. *Science*, **320**(5877), 769–772.
[14] Heller, W., Bockelmann, U. and Abstreiter, G. 1998. Electric-field effects on excitons in quantum dots. *Phys. Rev. B*, **57**(11), 6270–6273.
[15] Hennessy, K., Badolato, A., Winger, M. *et al.* 2007. Quantum nature of a strongly coupled single quantum dot-cavity system. *Nature (London)*, **445**(Feb), 896–899.
[16] Imamoğlu, A., Schmidt, H., Woods, G. and Deutsch, M. 1997. Strongly interacting photons in a nonlinear cavity. *Phys. Rev. Lett.*, **79**(8), 1467–1470.

[17] Imamoglu, A., Awschalom, D. D., Burkard, G. *et al.* 1999. Quantum information processing using quantum dot spins and cavity QED. *Phys. Rev. Lett.*, **83**(20), 4204–4207.
[18] Jalali, B. and Fathpour, S. 2006. Silicon photonics. *J. Lightwave Technol.*, **24**(12), 4600–4615.
[19] Joannopoulos, J. D. 1995. *Photonic Crystals: Molding the Flow of Light*. Princeton University Press.
[20] Kimble, H. J. 1994. *In Cavity Quantum Electrodynamics*, edited by P. Berman. San Diego: Academic Press.
[21] Kohmoto, S., Nakamura, H., Ishikawa, T. and Asakawa, K. 1999. Site-controlled self-organization of individual InAs quantum dots by scanning tunneling probe-assisted nanolithography. *Applied Physics Letters*, **75**(22), 3488–3490.
[22] Lee, J., Saucer, T. W., Martin, A. J. *et al.* 2011. Photoluminescence imaging of focused ion beam induced individual quantum dots. *Nano Letters*, **11**(3), 1040–1043.
[23] Loss, D. and DiVincenzo, D. P. 1998. Quantum computation with quantum dots. *Physical Review A*, **57**(1), 120–126.
[24] Michler, P. 2003. *Single Quantum Dots: Fundamentals, Applications, and New Concepts*. Springer-Verlag: Topics in Applied Physics.
[25] Miller, D. 2009. Device requirements for optical interconnects to silicon chips. *Proceedings of the IEEE*, **97**(7), 1166–1185.
[26] Noda, S. 2006. Recent progresses and future prospects of two- and three-dimensional photonic crystals. *J. Lightwave Tech.*, **24**(12), 4554–4567.
[27] Noda, S., Chutinan, A. and Imada, M. 2000. Trapping and emission of photons by a single defect in a photonic bandgap structure. *Nature*, **407**, 608–610.
[28] O'Brien, J. L., Furusawa, A. and Vučković, J. 2009. Photonic quantum technologies. *Nature Photonics*, **3**(12), 687–695.
[29] Ozbay, E. 2006. Plasmonics: merging photonics and electronics at nanoscale dimensions. *Science*, **311**(5758), 189–193.
[30] Press, D., Götzinger, S., Reitzenstein, S. *et al.* 2007. Photon antibunching from a single quantum-dot-microcavity system in the strong coupling regime. *Phys. Rev. Lett.*, **98**(11), 117402.
[31] Press, D., Ladd, T. D., Zhang, B. and Yamamoto, Y. 2008. Complete quantum control of a single quantum dot spin using ultrafast optical pulses. *Nature*, **456**(7219), 218–221.
[32] Purcell, E. M. 1946. Spontaneous emission probabilities at radio frequencies. *Physical Review*, **69**, 681.
[33] Santori, C., Fattal, D., and Yamamoto, Y. 2010. *Single-photon Devices and Applications*. Wiley-VCH.
[34] Schneider, C., Strauss, M., Sunner, T., *et al.* 2008. Lithographic alignment to site-controlled quantum dots for device integration. *Appl. Phys. Lett.*, **92**(18), 183101.
[35] Scully, M. O. and Zubairy, M. S. 1997. *Quantum Optics*. Cambridge: Cambridge University Press.
[36] Tan, S. M. 1999. A computational toolbox for quantum and atomic physics. *J. Opt. B*, **1**, 424–432.
[37] Thompson, R. J., Turchette, Q. A., Carnal, O. and Kimble, H. J. 1998. Nonlinear spectroscopy in the strong-coupling regime of cavity QED. *Phys. Rev. A*, **57**(4), 3084–3104.

[38] Thon, S. M., Rakher, M. T., Kim, H. *et al.* 2009. Strong coupling through optical positioning of a quantum dot in a photonic crystal cavity. *Appl. Phys. Lett.*, **94**(11), 111115.
[39] Vahala, K. J. 2003. Optical microcavities. *Nature*, **424**(6950), 839–846.
[40] Waks, E. and Vučković, J. 2006. Dipole induced transparency in drop-filter cavity-waveguide systems. *Phys. Rev. Lett.*, **96**(153601).
[41] Walls, D. F. and Milburn, G. J. 2008. *Quantum Optics*. Springer: Springer-Verlag Berlin Heidelberg.
[42] Yoshie, T., Scherer, A., Hendrickson, J. *et al.* 2004. Vacuum Rabi splitting with a single quantum dot in a photonic crystal nanocavity. *Nature*, **432**(Nov.), 200–203.
[43] Zwiller, V., Aichele, T., Hatami, F., Masselink, W. T. and Benson, O. 2005. Growth of single quantum dots on preprocessed structures: single photon emitters on a tip. *Appl. Phys. Lett.*, **86**(9), 091911.